1 **Quantification of major particulate matter species from a single filter type using**

2 **infrared spectroscopy – Application to a large-scale monitoring network**

3 Bruno Debus[1], Andrew T. Weakley[1], Satoshi Takahama[2], Kathryn M. George[1,3], Anahita Amiri

4 Farahani[1], Bret Schichtel[4], Scott Copeland[5], Anthony S. Wexler[1,6], Ann M. Dillner[1]*

5 [1] Air Quality Research Center, University of California, Davis, California, 95616, USA

6 [2] ENAC/IIE, Swiss Federal Institute of Technology Lausanne (EPFL), Lausanne, Switzerland

7 [3] Monitoring and Laboratory Division, California Air Resources Board, Sacramento, CA 95811,

8 USA

9 [4] National Park Service, Cooperative Institute for Research in the Atmosphere, Colorado State

10 University, Fort Collins, CO 80523, USA

11 [5] Cooperative Institute for Research in the Atmosphere, Colorado State University, Fort Collins,

12 CO, 80523, USA

13 [6] Departments of Mechanical and Aerospace Engineering, Civil and Environmental Engineering,

14 and Land, Air and Water Resources, University of California, Davis, California, 85616, USA

15 *Correspondence to:* Ann M. Dillner (amdillner@ucdavis.edu)

16 **Abstract**

17 To enable chemical speciation, monitoring networks collect particulate matter (PM) on different

18 filter media, each subjected to one or more analytical techniques to quantify PM composition

19 present in the atmosphere. In this work, we propose an alternate approach that uses one filter

20 type (teflon or polytetrafluoroethylene, PTFE, commonly used for aerosol sampling) and one

21 analytical method, Fourier Transform Infrared (FT-IR) spectroscopy to measure almost all of the

22 major constituents in the aerosol. In the proposed method, measurements using the typical

23 multi-filter, multi-analytical techniques are retained at a limited number of sites and used as

24 calibration standards. At all remaining sites, only sampling on PTFE and analysis by FT-IR is

25 performed. This method takes advantage of the sensitivity of the mid-IR domain to various

26 organic and inorganic functional groups and offers a fast and inexpensive way of exploring sample

27 composition. As a proof of concept, multiple years of samples collected within the Interagency

28 Monitoring of PROtected Visual Environment network (IMPROVE) are explored with the aim of

29 retaining high quality predictions for a broad range of atmospheric compounds including total

30 mass, organic (OC), elemental (EC) and total (TC) carbon, sulfate, nitrate and crustal elements.

31   Findings suggest that models based on only 21 sites, covering spatial and seasonal trends in
32   atmospheric composition, are stable over a three year period within the IMPROVE network with
33   acceptable prediction accuracy ($R^2 > 0.9$, median bias less than 3%) for most constituents. The
34   major limitation is measuring nitrate as it is known to volatilize off of PTFE filters. Incorporating
35   additional sites at low cost, partially replacing existing, more time and cost intensive techniques
36   or using the FT-IR data for quality control, are among the potential benefits of one-filter, one-
37   method approach.

1 Introduction

In the United States, filter-based chemical speciation of ambient aerosols has been in operation for decades to quantify trends, assess transport and atmospheric transformation, identify sources of air pollution, evaluate impacts of pollution regulations, assess impacts on visibility, radiative forcing, human and ecosystem health and evaluate atmospheric and climatological models. The two federally funded speciation networks, the Interagency Monitoring of PROtected Visual Environments (IMPROVE) and the Chemical Speciation Network (CSN) collect 24-hour filter samples using three filter media: polytetrafluoroethylene for analysis by gravimetry, hybrid integrating plate and sphere (HIPS), and x-ray fluorescence (XRF), quartz for thermal optical reflectance (TOR) and nylon for ion chromatography. Over the decades of operation, the analytical methods have evolved with efforts to maintain consistency in trends while also adopting improved methodology and retiring obsolete equipment. Impacts of many of these changes have been addressed in the literature (Hyslop et al., 2015, 2012; White et al., 2016; Zhang et al., 2021; Chow et al., 2007a, 2015) and in data advisories posted on the IMPROVE website (http://vista.cira.colostate.edu/Improve/data-advisories/).

In this paper, we explore the use of Fourier transform-infrared spectroscopy (FT-IR) to reproduce most of the existing speciation data based on the optical activity of the components in the mid-IR. The number and bands of organic compounds are numerous, but generally group frequencies can be found above 1500 cm^{-1} and compound-specific spectral patterns ("fingerprint region") below this frequency; down to approximately 700 cm^{-1} (for example, Weakley et al., 2016; Mayo et al., 2004). Graphitic carbon displays peaks near 1600 cm^{-1} due to lattice defects (Tuinstra and Koenig, 1970; Friedel and Carlson, 1971), displacement vibrations near 868 cm^{-1} (Nemanich et al., 1977), and a broad, sloping absorbance between 4000 and 1500 cm^{-1} due to the tail of the electronic transition more strongly observed in the UV (Parks et al., 2021). Inorganic substances containing polyatomic ions such as sulfate, nitrate, and ammonium have strong vibrational modes above 600 cm^{-1} (Mayo, 2004). Crystalline and amorphous geological minerals in the form of oxides (which include hydroxides and oxyhydroxides) have distinct internal vibrational modes influenced by the electronegativity of the metal to which the oxygen is bonded (Busca and Resini, 2006; Chukanov and Chervonnyi, 2016; Margenot et al., 2017).

FT-IR spectra with partial least squares (PLS) calibrations have been shown to reproduce OC and EC concentrations using organic and graphitic carbon absorption bands, respectively, at a limited number of sites in the IMPROVE network (Dillner and Takahama, 2015a, b; Reggente et al., 2016), CSN (Weakley et al., 2016, 2018a) and FRM (Weakley et al., 2018b). Takahama et al. (2019) reviews these findings and the overall framework to be used for the two phases of such statistical calibrations: model building (sample selection, spectral preparation, model generation, model selection, model evaluation, and model understanding) and operation (error anticipation and model updating).   Inorganic ions and geological mineral absorption bands have been used for

75 chemical speciation of these substances using FT-IR in prior studies (e.g., Cunningham et al.,
76 1974; McClenny et al., 1985; Pollard et al., 1990; Bogard et al., 1982; Foster and Walker, 1984).

77 Organic absorption bands are useful for measuring OC but also provide spectral information
78 needed to add detailed knowledge of composition not currently measured in air quality
79 monitoring networks – such as organic matter (OM) and organic functional group composition –
80 which is the subject of other work (Reggente et al., 2019; Boris et al., 2019, 2021; Burki et al.,
81 2020). Such calibrations, also combined with factor analytic approaches, can provide source
82 characterization on par with more costly mass spectrometric techniques (Boris et al., 2021;
83 Yazdani et al., 2021a; Hawkins et al., 2010; Takahama et al., 2011; Liu et al., 2012; Corrigan et al.,
84 2013).

85 Although FT-IR shows promise for measuring many constituents in aerosol, it is not without its
86 challenges. One limitation is that not all PM constituents can be measured, or measured with
87 high sensitivity, from the FT-IR spectrum. For instance, NaCl and $MgCl_2$ do not have IR-active
88 substituents. While a multitude of spectral signatures associated with mineral dust arise from
89 their constituent bonds – e.g., the metal-oxygen bonds in oxides (the oxide form is explicitly
90 assumed in estimating dust mass concentrations from elemental composition for the IMPROVE
91 network), some must be predicted from correlation with other constituents (e.g., some forms of
92 iron) if IR-activity is lacking. Other substances are IR-active but have weak responses, such as
93 graphitic carbon (Niyogi et al., 2006; Parks et al., 2021).   The absorption and scattering by the
94 PTFE filter also pose challenges for quantitative analysis. The PTFE-based material changes over
95 time due to change in manufacturer or manufacturing process, and is difficult to fully characterize
96 a priori or treat with simple blank subtraction techniques. PTFE absorption limits full access to
97 the range of spectroscopic information in the mid-IR, for instance in the region of carbon-oxygen
98 bonds that can lead to less than full recovery of OM mass. Additionally, scattering leads to
99 broadly-varying slope in the group frequency region. This scattering artifact is minimized by
100 baselining (Kuzmiakova et al., 2016) and using many standards that have a range of scattering
101 and absorption observed in the network (Debus et al., 2019), yet these techniques can still lead
102 to errors in quantification. Weakley et al., (2018b) demonstrated that calibrations built using one
103 brand of filter can be accurately extended to another brand of PTFE filter with numerically
104 marginal but statistically significant increase in method error (e.g., +2% error for $\alpha=0.05$).
105 However, these studies are insufficient to generalize findings to all types of sampling filters.

106 The goal of this work is to assess the capability of using FT-IR to measure the aerosol chemical
107 composition at all IMPROVE sites. FT-IR quickly and non-destructively collects information-rich
108 spectra from routinely collected PTFE filter samples. Ambient samples from strategically-
109 selected IMPROVE sites are used for calibration and reasonably mimic the composition, matrix
110 effects and substrates of the unknowns, all of which theoretically lead to accurate estimations of
111 concentrations. Using all samples from selected sites reduces maintenance, shipping, processing

112   and coordinating required to maintain intermittent quartz and nylon filter sampling at every site.
113   Sites are selected using data from 2015 and are used for calibrating samples from 2015-2017.
114   Samples from all other (non-calibration) IMPROVE sites are predicted and compared to routine
115   IMPROVE data to assess the quality of prediction. Aerosol components to be measured include
116   TC, OC, EC, inorganic ions, soil elements, particulate mass, and light absorption.

117 2   Methods

118 2.1   Network data

119   IMPROVE samples collected every third day at all North American sites (Section S1) from January
120   2015 through December 2017 are included in this study. Fine particulate matter (aerodynamic
121   diameter less than 2.5 micrometers) is deposited on 25 mm diameter filters
122   polytetrafluoroethylene (PTFE, Teflo, Pall Gelman) and quartz filters by sampling air at a nominal
123   flowrate of 22.8 liters per minute from midnight to midnight local time. Parallel 37 mm nylon
124   filters are collected at the same flow flowrate. PTFE filters are analyzed by multiple instruments
125   and archived for future analysis. Nylon filters and a portion of each quartz filter undergoes
126   destructive analysis and a remaining part of the quartz filters are retained for archive.

127   Over the period covered in this study, two different TOR instruments were employed to measure
128   OC, EC and TC. Quartz filters sampled prior to 2016 where analyzed on a DRI Model 2001 thermal
129   optical carbon analyzers (Chow et al., 1993) while filters collected beginning in January of 2016
130   were analyzed on a DRI Model 2015 multi-wavelength thermal optical carbon instrument (Magee
131   Scientific – Berkley, USA)(Chow et al., 2015). Both instruments use the IMPROVE_A protocol
132   (Chow et al., 2007b), which outlines the temperature step, gaseous environment in the
133   instrument and that reflectance is used to define the split point between OC and EC. To correct
134   for gas phase adsorption onto the quartz filter, the monthly median field blank OC concentration
135   is subtracted from each OC measurement during that sample month. Carbon concentrations are
136   reported in $\mu g/m^3$.

137   An in-house Hybrid Integrating Plate and Sphere (HIPS) system evaluates light absorption from
138   the PTFE filters in the IMPROVE network (White et al., 2016). In this work, the measured
139   absorption coefficient (*Fabs*) is converted into a TOR EC equivalent concentration assuming a
140   Fabs / EC ratio of 10 m^2g^{-1} (Malm et al., 1994). The resulting value, referred to as HIPS Black
141   Carbon (HIPS BC), is used as part of a quality control procedure to evaluate potential outliers in
142   TOR EC measurements.

143   Data from gravimetry and X-ray fluorescence (XRF) analysis obtained from PTFE filters and ion
144   chromatography from the nylon filters are also used in this study. Additional information on
145   routine IMPROVE methods can be found on the IMPROVE website
146   (http://vista.cira.colostate.edu/Improve/).   IMPROVE data are available online at
147   (http://views.cira.colostate.edu/fed).

2.2 Outlier removal

Data were screened for outliers to eliminate their influence on the results. Out of the ~61,500 total number of samples in the three-year period, fewer than 800 were excluded from the analysis due sampling issues or missing TOR, XRF or IC data. In addition, 65 samples collected at the Wheeler Peak Wilderness (New Mexico) site between November 2015 and April 2016 were excluded due to an EC contamination caused by a diesel-powered ski lift.

Potential outliers in TOR measurements were investigated by regressing TOR EC against HIPS BC concentrations. Samples with differences exceeding a predefined threshold value (0.68 $\mu g/m^3$) were flagged as potential outliers (section S2). The status of these samples was confirmed by building separate TOR EC and HIPS BC calibrations. The poor agreement between TOR EC and FT-IR EC concentrations contrasts with the nearly 1:1 relationship HIPS BC and FT-IR BC predicted values indicating that TOR EC concentrations were likely compromised (Section S2). For the period considered in this study, 112 samples with faulty TOR EC values were identified and excluded from further analysis. The number of valid sample spectra retained in this study is 61,462.

2.3 Fourier-transform infrared (FT-IR) analyses

Since 2015, all PTFE in the IMPROVE network have been analyzed by infrared spectroscopy for research and evaluation purposes. FT-IR measurement occurs after gravimetric analysis and prior to XRF and HIPS to prevent possible loss of volatile species under the mild vacuum in XRF. Three FT-IR spectrometers including one Tensor 27 and two Tensor 2 instruments (Bruker Optics, Billerica, MA) equipped with a pre-aligned mid-IR source and a liquid nitrogen-cooled wide-band mercury cadmium telluride (MCT) detector were used for spectra acquisition in the range 4000 - 420 cm^{-1} by averaging 512 scans at a nominal resolution of 4 cm^{-1}. The single beam signal associated with each PTFE filter was converted to an absorbance spectrum using the most recent zero reference signal, updated hourly.

Previously, it was determined that calibration transfer between multiple FT-IR instruments is not required as long as their spectral response is carefully matched by controlling a set of key environmental and instrumental parameters (Debus et al., 2019). Briefly, each mercury cadmium telluride (MCT) detector is connected to an automatic liquid nitrogen micro dosing system (NORHOF, Ede, Netherlands) designed to improve signal stability and maintain a high signal to noise ratio. The repeatability and reproducibility of the filter position relative to the IR beam is controlled via a house-built sample chamber (4.0 × 5.1 × 4.5 cm) mounted inside the instrument sample compartment. Details regarding the chamber design have been published elsewhere (Debus et al., 2019). Finally, the contribution of water vapor and carbon dioxide to the signal was minimized by continuously purging both the sample chamber and the optical bench with a VCD Series CO_2 adsorber / dryer system (PureGas LLC, Broomfield, CO). For each sample, the acquisition procedure involves a 4 minutes purge period followed by a spectrum collection lasting

185 about 1 minute. An in-house macro interfaced to the OPUS software (Bruker Optics, Billerica,
186 MA) controls each step. PTFE filters were measured in transmission mode without sample
187 preparation. No interpolated data (from zero-filling) are included in the final raw spectra.
188 Collected spectra are subjected to weekly quality control procedures detailed in (Debus et al.,
189 2019). Duplicate and replicate measurements were also performed to evaluate instrument
190 stability and found to be within +/- 10%.

191 ## 2.4   Multivariate Calibration Model - Partial Least Squares (PLS) Regression
192 While the presence of certain category of atmospheric compounds can be identified qualitatively
193 from an FT-IR spectrum, an accurate quantification of their concentration requires calibration.
194 PLS is a commonly used algorithm to relate a multi-wavenumber measurement to any particular
195 sample properties such as concentration (Wold et al., 2001). In brief, PLS maximizes the co-
196 variance between a set of response variables (species measurements) and a reference
197 measurement (FT-IR spectra) from which equivalent predicted values are desired. In so doing,
198 the optimal combination of response variables best describing the reference measurement is
199 identified and the selected features are used to build a multivariate calibration. With all least-
200 squares calibration methodologies, concentration-dependent biases in residuals that are
201 determined by the quality of fit (R^2) and dynamic range of the data are expected due to the nature
202 of least-squares estimation (Besalú et al., 2006; Draper and Smith, 1998, pp. 63-64,173,638). For
203 further discussion of these biases, see Section S1.

204 The applicability of PLS to quantify carbonaceous aerosol species (Reggente et al., 2016; Weakley
205 et al., 2016, 2018a) or functional groups (Boris et al., 2019; Ruthenburg et al., 2014) collected on
206 PTFE filters in various monitoring networks and field campaigns has been successfully
207 demonstrated. A complete review of the implementation of PLSR calibration in the framework
208 of atmospheric particulate matter characterization has been recently published (Takahama et al.,
209 2019).

210 To evaluate model performance, FT-IR predicted concentrations were regressed against their
211 reference measurement to quantify residuals and a series of metrics. Reported figures of merit
212 include the coefficient of determination (R^2), bias, error and the method detection limit (MDL).
213 Residuals are defined as the difference between predicted and reference concentrations, bias
214 corresponds to the median residual while error is the median absolute residual. To facilitate inter-
215 model comparison, relative performance metrics were calculated by normalizing the values by
216 their reference value. FT-IR PLSR calibration MDL was estimated from field blank predicted
217 concentrations as the 95th percentile minus the median residuals, as is done for other species in
218 the   IMPROVE   network   http://vista.cira.colostate.edu/improve/wp-
219 content/uploads/2021/07/IMPROVE-SOP-351_Data-Processing-and-Validation_2021_final.pdf.
220 Performance is reported for all samples together regardless if the samples were included in the
221 calibration. This enables comparison between models with different samples used for calibration.

222 For further insight into model prediction accuracy, the distribution in FT-IR residuals is
223 qualitatively compared with residuals from collocated measurements. Collocated quartz filters
224 are collected at the Everglades (FL), Hercules-Glades (MO), Medicine Lake (MT) and Phoenix (AZ)
225 sites. Similarly, collocated Teflon filters are sampled at Mesa Verde (CO), Proctor Maple Research
226 Facility (VT), Saint Marks National Wildlife Refuge (FL), Yosemite (CA) and Phoenix (AZ) sites while
227 collocated nylon filters are featured at the Phoenix (AZ), Frostburg Reservoir (MD), Mammoth
228 Cave (KY) and San Gabriel (CA) sites.

229 Data handling and analysis was performed in Matlab R2018a (The MatWorks, Inc, Natick, MA,
230 United States) using the statistics and signal processing toolboxes. PLS was computed via the
231 libPLS Matlab package (v1.9) (Li et al., 2018).

2.5   FT-IR Calibrations for Predicting PM Composition

233 This section presents the design of calibrations for quantifying the concentration of major
234 atmospheric species by taking advantage of the composition-based information embedded
235 within an FT-IR spectrum. In practice, spectra are calibrated against reference measurements
236 from TOR, XRF, IC, HIPS and gravimetric analysis with the aim of predicting concentrations of
237 atmospheric constituents using only spectra of PTFE filters as input.

238 A multilevel model (Snijders and Bosker, 2011; Takahama et al., 2019) is proposed in which
239 dedicated calibration models for subgroups of samples are constructed, and applied according
240 to a predetermined selection criterion for each sample. This model considers two subgroups: i)
241 samples determined to be dominated by biomass burning, which are calibrated with similar
242 samples, and ii) the remaining samples, which are calibrated with samples from a limited number
243 of sites.

244 To establish baseline performance metrics for comparison, a "Global model" in which a single
245 calibration (for each species) is constructed from all samples considered together is described in
246 Section S1 (Supplement).

247 The first step in the development of the Multilevel model consists of screening for biomass
248 burning samples. These samples are removed from consideration during the site selection
249 process. A simple detection method combining estimates of key functional group spectral peak
250 areas and spectral dissimilarity metrics were used to segregate biomass burning samples from all
251 other samples. Next, a Gaussian Mixture Model (GMM) was applied to the spectra of all non-
252 biomass burning samples. The GMM exploits the specificity of the infrared signal for organic and
253 inorganic species. The GMM was implemented with the aim of clustering the non-biomass
254 burning FT-IR spectra into groups sharing similar spectral features (Section 2.5.2). Those groups
255 were later used as part of the methodology for selecting sites with representative atmospheric
256 composition. Spectra from the year 2015 were used as a benchmark to validate the biomass
257 burning detection strategy, build the GMM and establish the list of representative sites where

258 multi-filter collection/multi-analyses should be retained (section 2.5.2). The identified biomass
259 burning samples are used to build a calibration for biomass burning samples (Section 2.5.1).

260 2.5.1 Biomass burning model
261 FT-IR spectra were used to estimate functional group areas and calculate spectral dissimilarities
262 metrics to segregate biomass burning samples from all other samples. Although this paper
263 focuses on using FT-IR to measure the major aerosol components in routine speciated aerosol
264 monitoring networks, FT-IR is more frequently used to measure organic functional groups (e.g.
265 (Russell et al., 2011; Ruthenburg et al., 2014; Boris et al., 2019). Specific regions in the IR spectra
266 correspond to specific functional groups. Peak areas, calculated from baseline corrected spectra
267 (see Section S3 for baseline procedure), for carbonyl, OH and CH were used rather than functional
268 group calibrations for simplicity. Because the relative functional group peak area tends to
269 increase significantly as the cumulative peak area decreases, typically for low mass deposition
270 samples, an estimate of spectral dissimilarities, the squared Mahalanobis distance (D_i^2), for each
271 site is also considered to minimize false detection. The Mahalanobis distance (Mahalanobis,
272 1936; Cios et al., 1998) is a measure of the spectral dissimilarity between a given spectrum at a
273 site and the mean spectrum at the site. Taking advantage of D_i^2 and relative functional group
274 areas, a set of criteria were established from observations at known wildfire sites during wildfire
275 season (O'Dell et al., 2019). First, samples collected under heavy smoke conditions whose spectra
276 fulfill C–H ≥ 2 %, C=O ≥ 15 % and $D_i^2 \geq 3\,\overline{D^2}$ were detected (Section S3). This group of spectra
277 tend to have large D_i^2 values and, consequently, the $3\,\overline{D^2}$ threshold often excludes samples with
278 low to moderate biomass burning contributions. For a more inclusive detection, spectra from the
279 first group were removed from consideration, the D_i^2 values are updated for each sample and
280 the plots were regenerated. The cut-off value for the relative carbonyl functional group area was
281 lowered to 8 % while other parameters were not changed. Spectra identified by the first and
282 second rounds are considered biomass burning samples. This procedure is performed for each
283 site and for each year of sample collection (Section S.3)

284 Recent work has shown that smoke samples may be identified using techniques such as cluster
285 analysis and labeling (Burki et al., 2020) similar to the GMM used here and through detection of
286 molecular markers – levoglucosan and lignin – or peak profiles in FT-IR spectra (Yazdani et al.,
287 2021a, b). For the large data set in this work (~20,000 samples in 2015), cluster analysis
288 resulted in multiple clusters that could be associated with smoke-impacted samples likely due
289 to the variations in fuel, oxidation conditions, and contributions from other sources. Therefore,
290 for this work we selected a single group of smoke-impacted samples based on specific organic
291 features known to be present in FT-IR spectra. While the criteria for smoke-impact labeling can
292 be defined differently according to each intended purpose, the method presented here is
293 demonstrated to sufficiently partition the samples for building accurate submodels to predict
294 concentrations of PM constituents.

295 While ions and crustal species are not necessary correlated with wildfire emissions, the Biomass
296 Burning sub-model accounts for interferences that are necessary to track in order to maintain
297 high prediction accuracy for samples collected on smoky days.

2.5.2 Limited Sites Model

299 To assess major PM$_{2.5}$ composition regimes in the network and to identify representative sites to
300 use as calibration standards in the Limited Sites model, screening of all FT-IR spectra (except
301 samples identified as biomass burning samples) across all locations and seasons was performed
302 by building a Gaussian Mixture Model (GMM) (Bilmes, J. A., 1998; Hastie, T et al., 2009). The basic
303 idea behind GMM is to group FT-IR spectra into clusters of similar spectral shape using a
304 probabilistic approach describing the likelihood that any given spectrum belongs to a particular
305 class. To minimize the concentration dependence and emphasize composition, raw spectra were
306 transformed to second derivative spectra using a 2nd order, 21 point, Savitzky-Golay filter
307 (Savitzky and Golay, 1964), differenced with filter blank spectra and divided by their respective
308 Euclidean norm (Bro and Smilde, 2003). Additional details about the GMM pre-processing and
309 implementation as well as cluster interpretation are provided in Section S4.

310 After classification, a single site per cluster was selected to represent the atmospheric
311 composition captured in that cluster. For any given cluster, the retained location was defined as
312 the site with the largest number of classified spectra with the highest probabilities of belonging
313 to that cluster. To prevent misleading site selection and enhance spatial coverage, the following
314 set of decision rules were used: *i)* if the same site is representative of two clusters, it is ascribed
315 to the cluster with the largest number of classified spectra from that site, *ii)* if none of the
316 retained sites accounts for a given spatial region or known source type in the network, an
317 additional site with the highest number of classified spectra is selected from a nearby cluster,
318 and *iii)* only sites under continuous operation between 2015 and 2017 are eligible for selection.
319 Criteria *ii)* was invoked once to add a site in the Midwest to improve spatial coverage in that
320 region and to capture prescribed fire emissions in Kansas. All non-biomass burning samples from
321 selected sites were used as FT-IR calibration standards for all species and all non-biomass burning
322 samples are predicted with these models. Once established, the selected sites are not re-
323 evaluated but instead were used in all subsequent years as would occur in practice.

2.5.3 Application of Multilevel Model

325 The Multilevel model is the combined FT-IR predicted concentrations from the Limited sites and
326 Biomass burning models. Multilevel modeling will be discussed in the context of carbonaceous
327 aerosols before extending the modeling to other atmospheric constituents with detectable
328 infrared signatures. In addition to OC and EC, species evaluated for FT-IR prediction include PM$_{2.5}$
329 mass, soil elements (silicon, aluminum, calcium, titanium, iron), anions (sulfate, nitrate) and HIPS
330 BC. As mentioned previously, NaCl is not IR active and so there is no direct measure of seasalt
331 from FT-IR. Next, the years 2016 and 2017 will be examined to assess the long-term stability of

332 the proposed Multilevel strategy by screening for smoke samples and re-calibrating each year
333 using the sites selected using 2015 data.

3   Results and discussion

335 In the following sections, the quality of FT-IR based calibrations for quantifying aerosol
336 composition across continental US and their long-term applicability to large speciation
337 monitoring networks will be assessed. Section 3.1 describes the selected calibration samples for
338 the Biomass Burning and Limited Sites models. In Section 3.2, Biomass Burning and Limited
339 model performance will be briefly reviewed before exploring the Multilevel FT-IR predictions for
340 all samples. Initially focused on carbonaceous species on PTFE samples collected in 2015, FT-IR
341 predictions will be extended to other atmospheric constituents and years.

3.1   Multilevel modeling – Calibration sample selection

3.1.1   Biomass burning sample selection

344 Using the methods described above, 492 samples impacted by biomass burning emissions were
345 identified in 2015 (2.5 % of the network), 288 samples in 2016 (1.5 %), and 817 samples in 2017
346 (3.7 %). The mean OC concentration of the biomass burning samples range was 5.6 – 8.3 μg/m^3
347 with maximum concentrations extending from 44 to 97 μg/m^3 over the three year period.
348 Similarly, per year, the mean EC concentration varies between 0.6 – 0.9 μg/m^3 with maximums
349 up to 2.9 – 3.9 μg/m^3. Mean OC/EC ratios are larger than 7, in agreement with past literature
350 (Schichtel et al., 2008; Sorooshian et al., 2011). Analysis of the detected samples shows reliable
351 spatial and seasonal distributions, consistent with biomass burning emissions predominantly in
352 summer and fall across the Pacific North West and Northwestern US (Section S3). Two-thirds of
353 the identified samples were selected (Section S5) as calibration standards for the calibration and
354 resulting model was applied to the remaining third of the smoke impacted samples.

3.1.2   Limited Sites model – clusters and retained sites

356 Figure 1 shows the spatial distribution and annual average composition (from routine IMPROVE
357 data) of the 21 sites selected for the Limited sites model calibratoin. From a spatial standpoint,
358 retained sites appear reasonably scattered across the network including Hawaii and the Virgin
359 Islands. Clusters are represented by a distribution of urban and rural sites. One urban cluster is
360 represented by Fresno and contains mostly urban samples from Fresno and Phoenix. All other
361 clusters contain mostly rural and pristine sites. However, two other urban sites were retained,
362 Phoenix and Birmingham. The Phoenix cluster contains samples from the southwest in the
363 spring. The Birmingham site along with the Tallgrass site represent a non-western cluster in the
364 spring and summer.
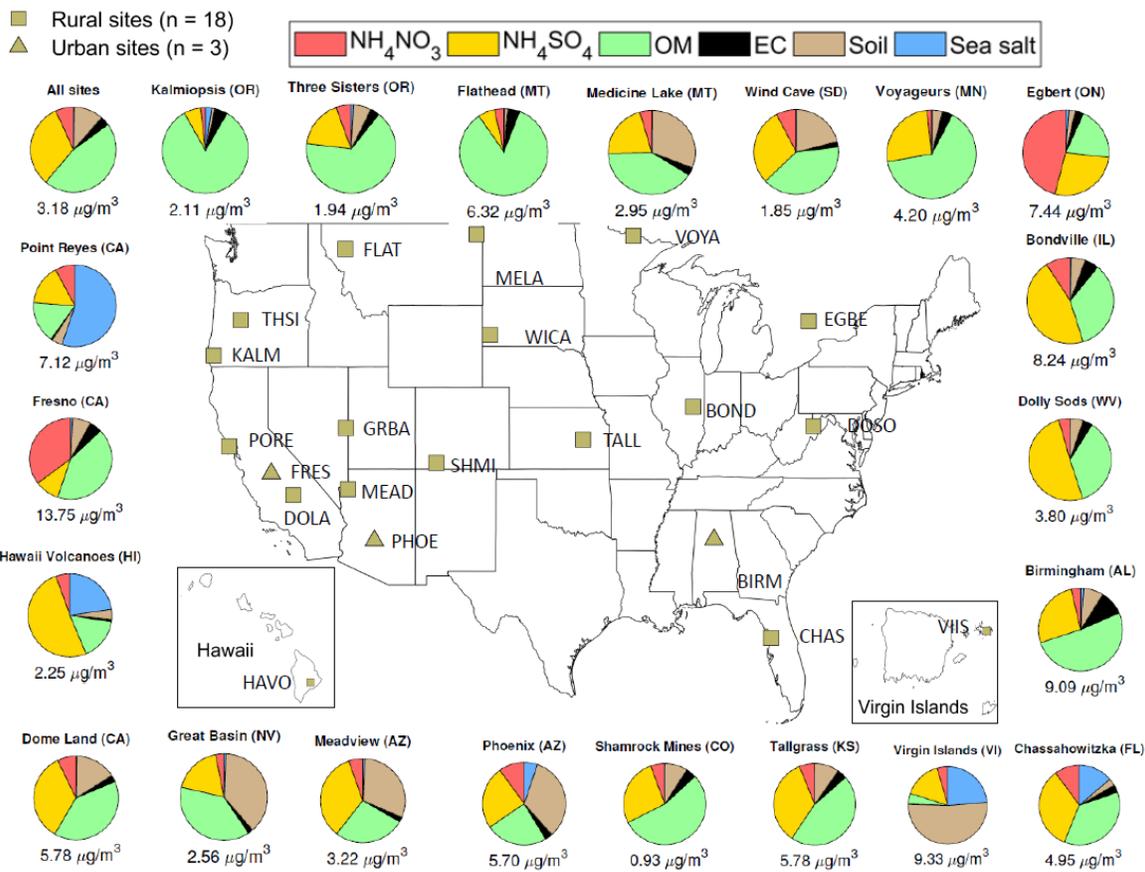
Figure 1: Spatial distribution, median PM$_{2.5}$ concentration and composition of the 21 representative sites. The composition is obtained from routine IMPROVE (non-FT-IR) measurements and the IMPROVE reconstructed fine mass equation (http://vista.cira.colostate.edu/Improve/reconstructed-fine-mass/) to calculate soil and seasalt. Sites are identified by the four letter site code which is the first four letters of a single word site name (Fresno = FRES) or the first two letters of the first and second word for two word site names (Dome Land = DOLA). The top left pie chart representing the median PM$_{2.5}$ composition across all sites and samples is given for comparison.

The clusters are also seasonally distributed (Section S6): five clusters are dominated by fall - winter samples, ten clusters containing summer samples (along with varying number of spring and fall samples), two clusters are predominately spring and one is spring - fall. Three clusters have little seasonality.

379 Because FT-IR spectra are clustered based on composition, the first step in assessing the
380 representativeness of the 21 sites is to compare the concentration ranges. For this purpose,
381 distributions in TOR OC and EC concentrations excluding biomass burning samples are compared
382 for the 21 sites used for calibration and the 140 remaining sites. In Fig. 2, the two probability
383 density functions are very similar for both OC and EC despite large differences in sample
384 populations (2572 and 16,543, respectively). In addition to matching the range of carbonaceous
385 concentrations observed in the rest of the network, the presence of species interfering with
386 organic functional groups should also be accounted for by the calibration. Because ammonium
387 absorptions overlap with carbonaceous absorptions, situations where ammonium to OC and
388 ammonium to EC ratios are different between calibration samples and samples to be predicted
389 were associated with additional sources of bias and error (Dillner and Takahama, 2015a, b).
390 Although not measured in IMPROVE, ammonium concentration is approximated from nitrate and
391 sulfate assuming both species are fully neutralized. The corresponding probability distribution in
392 Fig. 2 confirms the equivalence between the ranges of ammonium/OC and ammonium/EC
393 concentrations spanned by the Limited sites samples and the overall network. In section S6, Fig.
394 S6-3 shows reasonable agreement between the selected sites and the rest of the network for
395 PM2.5 mass, ions, elements and HIPS BC. Together, these results suggest the list of 21 sites is a
396 suitable representation of network variations in OC and EC and their relative proportion to
397 ammonium, and for all other predicted constituents.
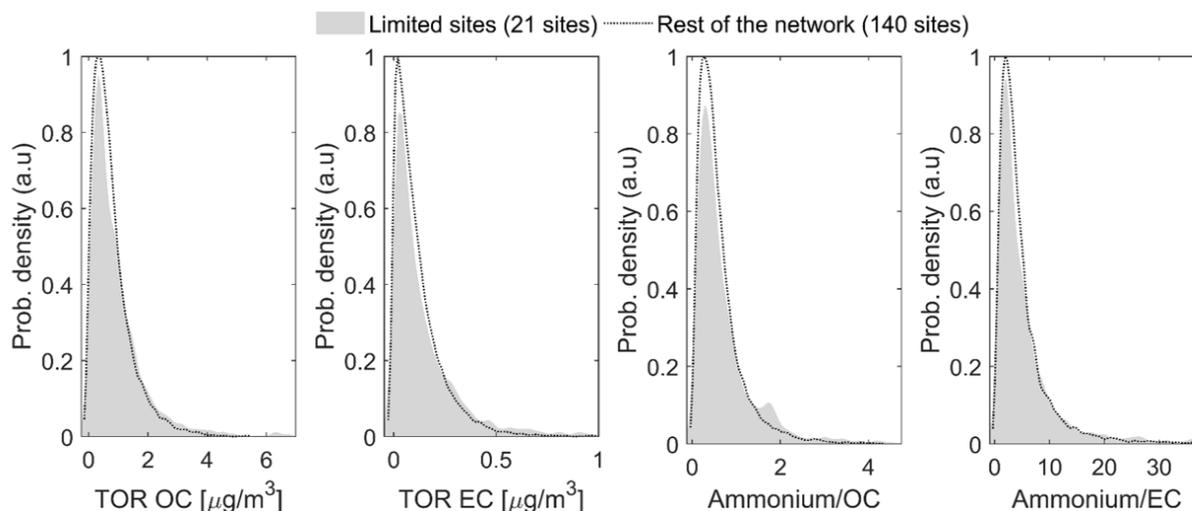
399 **Figure 2**: Comparison of probability density function for OC, EC and ammonium concentrations
400 in 2015 between the 21 sites retained for Limited calibration and the rest of the network.

401 The spatial and seasonal as well as the urban and rural diversity supports the compositional
402 diversity of the selected sites as shown in Fig. 1.   The three urban sites have distinct
403 characteristics. At the Fresno, CA site, the composition is dominated by nitrate (35 %) and organic

404   matter (42 %) with an autumn – winter pattern consistent with agriculture and residential wood
405   burning activities (Ngo et al., 2010) as well as with the formation of secondary aerosols during
406   stagnation events and a low inversion layer (Watson and Chow, 2002). Phoenix, AZ site features
407   a strong soil component (33%) associated with spring dust storms and windblown dust and equal
408   proportions of ammonium sulfate (25 %) and OM (24 %) occurring mostly in spring and summer.
409   The ammonium sulfate and organic matter has been attributed to regional power production and
410   traffic (Brown et al. 2007). In contrast, Birmingham samples show little seasonal trend with
411   elevated OM (52 %) and EC (10 %) fractions originating from various combustion processes
412   including vehicle exhaust, biomass burning and biogenic secondary organic aerosols (Blanchard
413   et al. 2016). The other dominant species at this site is ammonium sulfate (26 %), characteristic of
414   coal burning and industrial activities in the East (Watson et al. 2015).

415   Among rural sites, four noticeable patterns in $PM_{2.5}$ composition are distinguishable. The first
416   corresponds to OM fractions accounting for more than two-thirds of the filter mass. High OM
417   samples are encountered at four locations in Northwestern US, namely the Kalmiopsis (OR),
418   Three Sisters (OR), Flathead (MT) and Voyageurs (MT) sites. Samples from Voyageurs (MN) and
419   Flathead (MT) sites are from Summer-Fall and present elevated median $PM_{2.5}$ concentrations
420   (4.20 $\mu g/m^3$ and 6.32 $\mu g/m^3$, respectively) and very large percentage of OM consistent with
421   biomass burning emissions. Kalmiopsis (OR) and Three Sisters (OR) samples have a lower and
422   nearly identical median $PM_{2.5}$ concentration (≈ 2 $\mu g/m^3$) but differ in their monthly distribution
423   with the former displaying more winter samples than any other season whereas the later shows
424   little seasonality.

425   The second type of sites have high OM and sulfate concentrations. Both Shamrock Mines (CO)
426   and Tallgrass Prairie (KS) sites have larger OM than sulfate content. However, the Colorado site
427   has more autumn – winter samples, represents samples in the Rockies and Alaska and an overall
428   small median $PM_{2.5}$ concentration (< 1 $\mu g/m^3$). The Kansas site has a majority of spring samples,
429   representing non-western samples and has a significantly larger $PM_{2.5}$ concentration (≈ 6 $\mu g/m^3$)
430   that is attributed to prescribed burning near the Tallgrass site (Whitehill et al. 2019). Other sites
431   have higher median sulfate concentrations (~50%) than OM concentrations (~40%) such as Dolly
432   Sods (WV) and Bondville (IL). The monthly sample distribution indicates seasonal influences:
433   Bondville (IL) samples are mostly from the summer and the concentrations are relatively high
434   while the Dolly Sods (WV) site samples are mostly not in the summer with lower concentrations.
435   Because the spectra were normalized to minimize influence of concentration, these two clusters
436   likely have different organic composition even though the relative amount of OM is the same.
437   Finally, situations where sulfate and OM are present in equal proportions (≈ 36 %) are reported
438   at the Dome Land (CA) and Chassahowitzka (FL) pristine sites mainly featuring spring – summer
439   and winter samples, respectively.

440   A third group of noteworthy PM$_{2.5}$ compositions at rural sites contain a large fraction of (> 20 %
441   of the total mass). The Virgin Islands (VI) site presents the highest soil fraction across the network
442   52 % of the total PM$_{2.5}$ mass, mostly originating from long-range Sahara soil dust transport
443   (Holmes and Miller 2004). In addition to sulfate and OM, elevated soil contributions are observed
444   for the Wind Cave (SD), Meadview (AZ), Medicine Lake (MT), and Great Basin (NV) sites with soil
445   content between 20 and 40%. Although the seasonality is somewhat different between these
446   sites, they all have many samples from the spring suggesting the dust is due at least in part to
447   spring dust storms and may also contain resuspended road dust and more localized dust sources.

448   A fourth and final distinct category of PM$_{2.5}$ composition includes a collection of sites with unique
449   local atmospheric pollution sources, specific to those locations. The Hawaii Volcanoes (HI) site
450   where sulfur emitted as part as the volcanic activity, contains 51% sulfate along with sea salt (23
451   %). Another location with unique composition is the Point Reyes (CA) site where the sea salt
452   contribution reaches 55% of the median filter mass for the clustered samples, larger than any
453   other marine site in the network. Finally, the Egbert (ON) Canadian site, representing the upper
454   Midwest in winter is dominated by nitrate (46 %), sulfate (27 %) and OM (20 %).

455   As described above, the 21 sites retained for the Limited sites sub-calibration present seasonal,
456   regional and compositional features consistent with known or expected trends in PM$_{2.5}$ across
457   the network. The median PM$_{2.5}$ mass at those locations covers a broad range of concentrations
458   ranging from 0.93 μg/m^3 to 13.75 μg/m^3 and includes both urban and rural sites. Capturing the
459   large variability in PM$_{2.5}$ composition and concentration is essential to ensure the proposed site
460   list is a representative subset of the parent network. However, it should be mentioned that the
461   proposed site list is not unique but is one of the many feasible solutions since sites whose samples
462   clustered together in the GMM are likely inter-exchangeable.

3.2   Evaluation of Biomass Burning Model

463

464   Prior to describing the overall results from the Multilevel model, the Biomass Burning model is
465   evaluated to determine if the biomass burning model improves predictions for those samples.
466   To evaluate the quality of the biomass burning model, the predictions are compared to a global
467   model (section S1) which contains a few samples from all 160 sites which are mostly non-smoke
468   samples but does contain a few smoke samples. Visual inspection of Fig. 3 suggests the
469   equivalence of the biomass burning models to the global model at the lower end of the
470   concentration range. However, improvement in prediction accuracy can be claimed at high
471   concentrations for the Biomass Burning model. The gain in model performance is subtle for OC
472   and TC; however, for EC, predictions benefit from having a dedicated calibration for samples
473   impacted by wildfire emissions, with an increase in R^2 from 0.747 to 0.902 (Section S7).
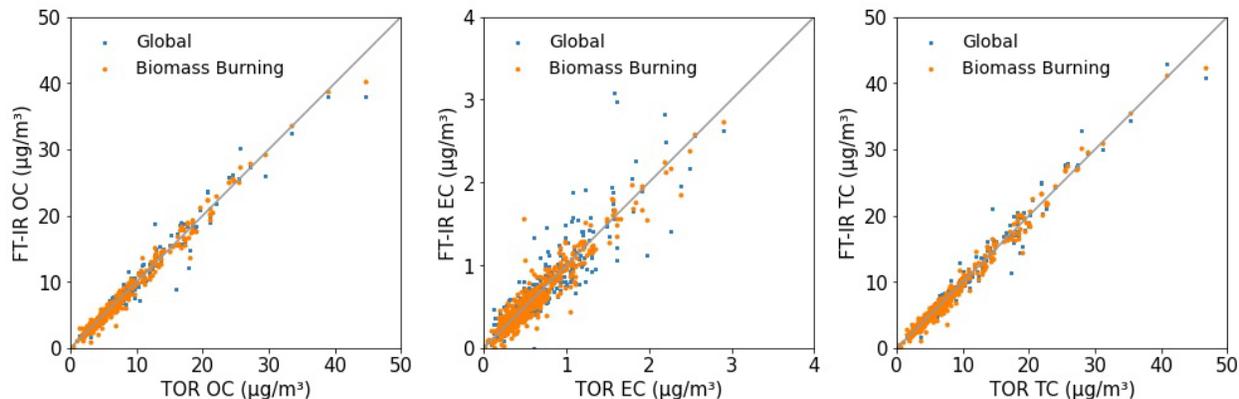
Figure 3: Inter-model OC (left), EC (middle), TC (right) comparison between global (section S1) and Biomass Burning predicted concentrations for the 492 samples classified as biomass burning in 2015. EC prediction, in particular, benefit from having a dedicated Biomass Burning calibration model.

Therefore, we retain the biomass burning model as part of the multilevel model and present the results for the Multilevel model below.

3.3   Multilevel modeling – Performance evaluation

3.3.1 Carbonaceous aerosol predictions

Figure 4 shows the correspondence between FT-IR Multilevel concentrations for OC and EC and TOR measurements for 2015 (plot for TC can be found in Section S9) and Table 1 lists the prediction metrics for all 3 carbonaceous components. The visual agreement between FT-IR and the reference measurements of OC and EC is high but EC shows higher scatter than the other measurements. Table 1 indicates that FT-IR OC and TC has higher prediction quality than EC but both perform satisfactorily. FT-IR OC and TC error is on par with TOR precisions (Table 1) indicating that on average FT-IR does not add significant additional error to the measurement. FT-IR EC predictions, however, have higher error than TOR precision. With respect to reference (TOR) measurements, concentration-dependent biases in residuals that are determined by the quality of fit (R^2) and dynamic range of the data are expected due to the nature of least-squares estimation (Besalú et al., 2006; Draper and Smith, 1998). For bias defined as FT-IR predictions minus the reference (TOR) measurement, least-squares estimator causes an apparent linear bias which is positive at the low end of the concentration range and negative at the high end of the concentration range (see Section S8 for further discussion). The satisfactory agreement between FT-IR and TOR concentrations as well as the equivalence agreements using the global model (Section S1) support the validity of the proposed Multilevel modeling in the context of carbonaceous aerosols prediction from PTFE filters in large speciation networks.
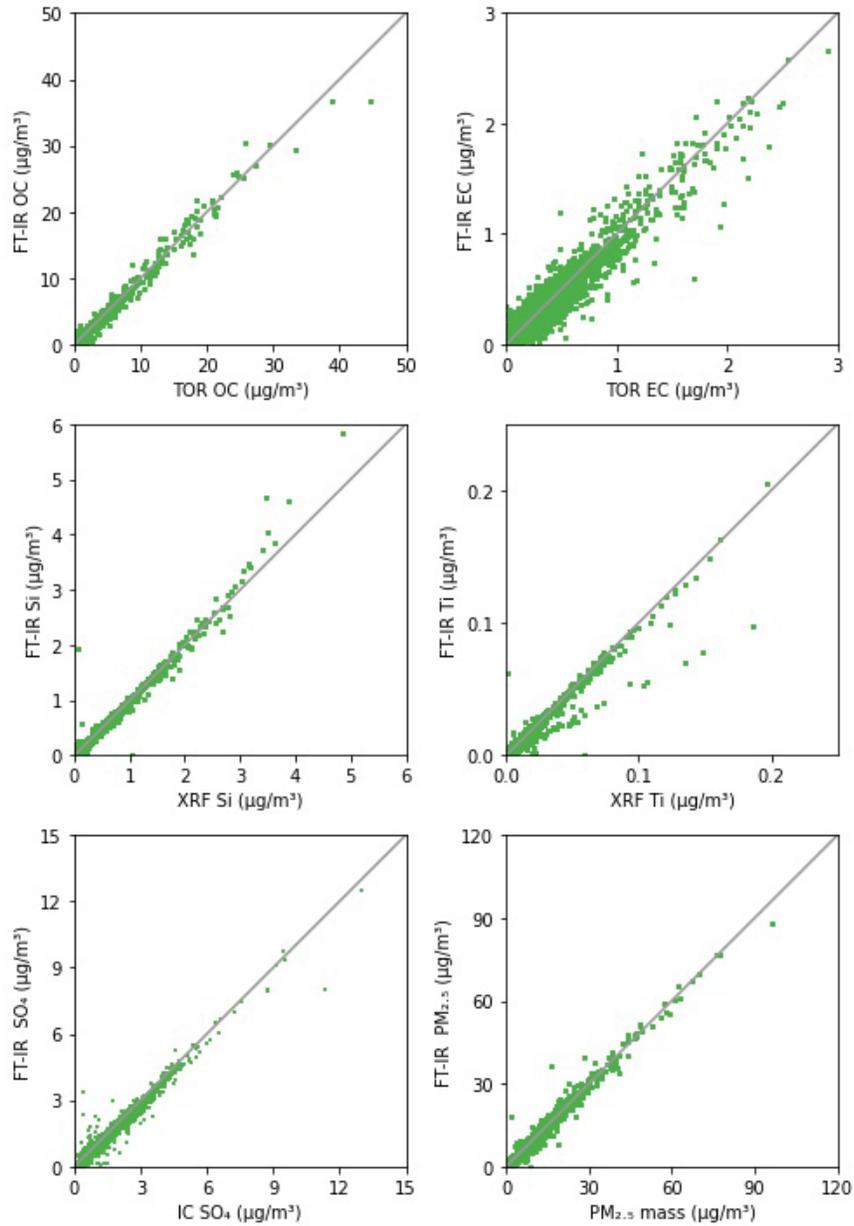
501 **Figure 4**: Comparison of predicted FT-IR OC, EC, Si, Ti, SO₄ and mass concentrations using the
502 Multilevel model against their reference measurements. Each subplot contains all 19,608
503 samples collected in the year 2015.

504

505 **Table 1**: Summary of Multilevel model performance for IR-active atmospheric constituents for
506 19,608 spectra analyzed by FT-IR in the year 2015.

Species	R^2	Bias [μg/m³]	Bias (%)	Error [μg/m³]	Error (%)	Reference Data Error[1] (%)	MDL [μg/m³]	< MDL (%)
OC	0.983	0.01	1.6	0.08	12	10	0.06	0.9
EC	0.912	0	1.7	0.02	30	15	0.04	20.7
TC	0.984	0.01	1.2	0.08	12	11	0.07	1.3
BC	0.92	0	-0.3	0.03	23	---	0.04	19.3
Si	0.983	0	2.2	0.01	11	13	0.01	9.7
Al	0.985	0	2.2	0	12	10	0	4.7
Ca	0.979	0	1.1	0	13	9	0	6.9
Ti	0.941	0	2.7	0	21	16	0	14.9
Fe	0.95	0	1.1	0	25	8	0.01	19
SO$_4$	0.983	0	0.1	0.03	6	2	0.03	0.9
NO$_3$	0.927	0.02	15.3	0.07	54	8	0.07	21.8
PM$_{2.5}$ Mass	0.985	0.03	1	0.18	6	6	0.25	1.1

507 [1]Median relative error for TOR, XRF, IC and gravimetric analysis. OC, EC and TC median relative error estimated
508 from collocated sampling as measurement error/uncertainty is not reported by IMPROVE for this components.
509 For all other components, the normalized error was calculated as the uncertainty divided by the concentration
510 prior to selecting the median. BC is not reported by IMPROVE so measurement error is not estimated.

511 In addition to OC, EC and TC, light absorption which is predominantly due to black carbon, is also
512 a measure of one fraction of the carbonaceous aerosol. FT-IR calibrations are found to be
513 adequate for replicating HIPS BC measurements (Section S9). As expected, the corresponding
514 model is similar in performance to EC with R^2 and relative error of 0.920 and 23.3 %, respectively
515 (Table 1). FT-IR BC residuals have a broader interquartile range than in the HIPS BC collocated
516 data (Section S9). We attribute this effect to a difference in signal to noise ratio and sensitivity to
517 chemical interferents between the two analytical techniques. While HIPS exploits the strong
518 absorption properties of refractory carbon in the visible domain, the weak absorptivity of EC in
519 the mid-infrared domain (Niyogi et al., 2006) and the presence of overlapping species makes the
520 quantification less accurate.

521 Further exploration of the regional and site by site quality of data is made via contiguous United
522 States (CONUS) maps of annual median reference method concentrations (left), difference in %
523 below MDL between FTIR and reference method (middle) and relative error (right) are shown in
524 Figure 5 for OC and EC. TC is very similar to OC and BC is very similar to EC.

525   Maps for all constituents with annual median FTIR and reference method concentrations, as well
526   as annual median prediction metrics are shown in Section S10.

527
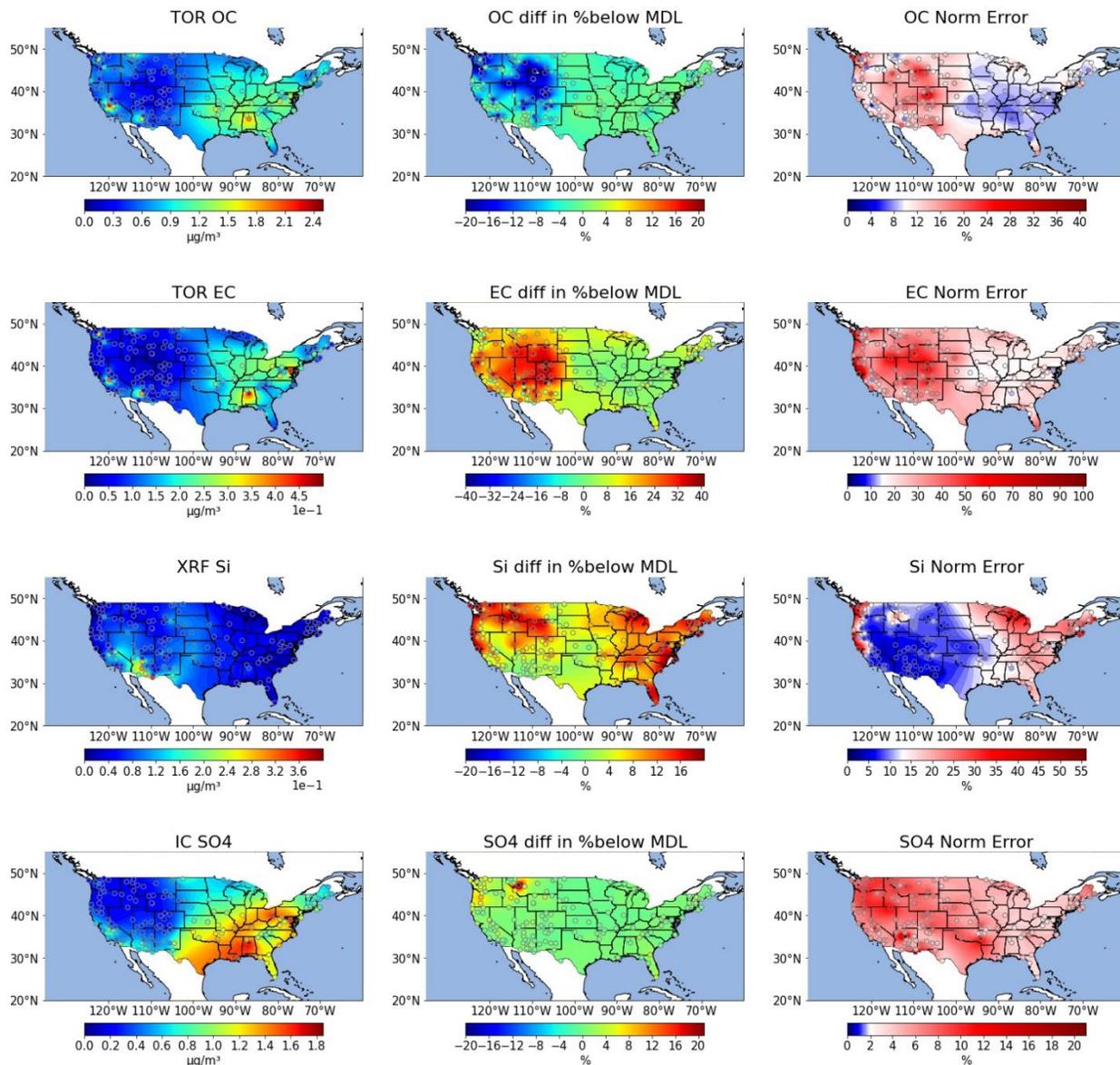
Figure 5. Annual median reference method concentrations (left), difference in % below MDL (middle) and normalized relative error (right) per site for OC, EC, silicon, and sulfate for CONUS for 2015. For the MDL plot, sites in green and blue indicate that the FTIR has the same of fewer samples below MDL than the reference method. Sites in yellow and red have more samples below MDL for FTIR than for the reference method. For the relative error maps, the median relative error of the reference method estimated using methods described in Table 1 is white. For sites in blue, FTIR has lower relative error than the reference method and sites in red are higher.

537 Annual median maps of FT-IR OC and TOR OC as well as maps of FT-IR EC and TOR EC
538 (Supplemental material S10) are nearly identical. As shown in Figure 5, annual median OC and
539 EC concentrations are highest at the four urban IMPROVE sites of Seattle, WA, Fresno, CA,
540 Phoenix, AZ and Birmingham, AL than the rural sites and are higher in the east than in the west.
541 For OC, the relative error is lower than the TOR relative error in the east (where concentrations
542 are higher) and higher than TOR relative error in the west. OC has an equal or lower number of
543 samples below MDL than TOR at all sites. For EC, FTIR relative error is higher than TOR relative
544 error at almost all sites. The percentage of samples of EC that are below MDL for FTIR is similar
545 to are slightly higher than TOR in the eastern US where EC concentrations are higher and are
546 significantly higher than TOR in the western US where concentrations are lower. These
547 patterns indicate that FTIR does not add error to OC measurements when concentrations are
548 above 0.75 μg/m^3 but does add some error at lower OC concentrations and for EC
549 measurements.

550 ### 3.3.2   Elemental oxide predictions
551
552 Taking advantage of known mineral absorbance bands in the mid-infrared range (Hahn et al.,
553 2018; Madejová and Komadel, 2001; Senthil Kumar and Rajkumar, 2013) (Section S9), Multilevel
554 calibrations for soil elements were evaluated for the five crustal elements commonly used to
555 estimate soil: silicon, aluminum, calcium, titanium, and iron (Table 1 and Fig. 4 for Si and Ti). All
556 models present a satisfactory agreement between XRF and FT-IR predicted concentrations (R^2 >
557 0.94).   The quality of prediction of the elemental oxides falls into two groups. The first group
558 includes silicon, aluminum and calcium and is characterized by moderate relative errors (11 – 13
559 %), similar in magnitude to the FT-IR OC model (12 %) and have similar errors to XRF
560 measurements. This indicates that like OC and TC, on-average FT-IR does not add additional
561 uncertainty. The second group includes titanium and iron which have larger relative errors (20.9
562 – 24.8 %), analogous to HIPS BC and EC models (23.3 – 30 %). Comparing residuals to collocated
563 XRF measurements (Section S9) shows that the FT-IR based models have a larger interquartile
564 range. For Fe, XRF uncertainty is quite low and FT-IR adds additional uncertainty to the
565 measurement. XRF Ti measurements have higher error than the other elements but there is an
566 incremental increase in error due to FT-IR. In addition, cross plots of titanium concentrations
567 show a bifurcation (Fig. 4). While most samples fall near their expected titanium concentration,
568 samples collected at the Sycamore Canyon (AZ) site present a systematic negative bias, consistent
569 across years, tentatively attributed to a site-specific soil composition not accounted for by the
570 Limited calibration. Takahama et al. (2019) demonstrated several methods to identify the
571 possible occurrence of anomalous predictions in OC and EC based on comparison of new sample
572 spectra to calibration spectra based on projected PLS scores and regression residual vectors.

573   These samples with systematic negative bias in titanium predictions can presumably be identified
574   using such an approach, provided that compositional differences are detected in the IR spectrum.
575   Although distinct IR fingerprints exist, FT-IR calibrations for quantifying mineral contents should
576   be interpreted with care as specific elements may be indirectly quantified through their
577   correlation with another element even in the absence of clear IR signature (Hahn et al., 2018).
578   For instance, the variable importance in projection (VIP) scores for the Si, Al, and Ti calibrations
579   suggests use of similar spectral variables, with small differences, for prediction of these species
580   (Section S9). However, the 21 GMM sites coverage still meet the necessary requirements for
581   providing a reliable insight into soil composition in the IMPROVE network.

582   Figure 5 shows the distribution of concentrations of XRF Si across CONUS. The highest annual
583   median concentrations are in the southwest. Similar patterns are found for Al, Ca, Ti and Fe
584   except that high Fe concentrations are also observed at the urban sites, particularly Fresno, CA
585   and Birmingham, AL (Figures S10-6 through S10-9). For Si, FTIR normalized error is lower than
586   XRF in the west where concentrations are higher. For Ca, Ti and Al, FT-IR normalized error is
587   lower only in the southwest. For Fe, FT-IR is above XRF normalized error. The percentage of
588   samples below MDL are similar to XRF (0-10% different) in the southwest and central US and
589   modestly higher (15-20%) in the northwest and eastern US for Si. For Fe, the spatial pattern is
590   similar but the FTIR % below MDL is up to 50 % higher than XRF. However, for Al, Ca, and Ti, FTIR
591   percent below MDL is approximately the same or lower than XRF at all sites.

592   ### 3.3.3   Inorganic ions

593   The two most abundant inorganic anions quantified in the network: nitrate and sulfate can also
594   be measured by FT-IR (absorption bands used for prediction are discussed in Section S9). FT-IR
595   sulfate concentrations display a satisfactory agreement with the reference IR measurements
596   (Fig. 4). Model performance metrics include R^2 above 0.98 and relative error of 6 %. The relative
597   error is the same as for FT-IR $PM_{2.5}$ and lower than OC, TC, and Si (Table 1). However, IC
598   measurements have even lower error than FT-IR sulfate. Compared to sulfate, FT-IR nitrate
599   concentrations (Section S9) are characterized by a moderate drop in the overall model
600   performance (R^2 = 0.927) while relative bias and error exceed 15 % and 50 %, respectively and
601   the error far exceeds reference IC nitrate measurement error. A direct comparison against
602   differential nitrate concentrations at collocated sites highlights the broad uncertainty in
603   determining nitrate content from PTFE filters (Section S9, Figure S9-3). Unlike nylon filters for
604   which nitrate is trapped on the surface, nitrate is known to evaporate from PTFE filters and the
605   extent of volatilization is dependent on temperature and relative humidity during and after
606   sampling. This causes a discrepancy between the mass of nitrate deposited onto the nylon filter
607   and the mass of nitrate on the PTFE filter (Eldred and Ashbaugh, 2004), therefore FT-IR
608   calibrations with the nitrate measurements by IC from nylon filters as the reference should be
609   used with caution. Although there are physical limitations to measuring ambient nitrate on

610 PTFE filters, a measure of nitrate on PTFE filters which corresponds to its contribution to the
611 gravimetric mass is useful for mass closure and data validation. FT-IR has been shown to be
612 useful for measuring and evaluating nitrate under controlled laboratory conditions (ex. Wu et
613 al., 2007). For network samples, nitrate could be measured using laboratory calibration
614 standards and this effort will be addressed in future work.

615 The annual median sulfate concentration by IC is shown in Figure 5. Annual median
616 concentrations are highest in the southeast and eastern US with a gradient in concentrations
617 observed across the midwest. The median relative error for sulfate by IC is only 2% and all FTIR
618 sulfate has higher relative error. There are however, spatial differences. In the eastern US
619 sulfate relative error is less than 15% but in the west, it is considerably higher, peaking in
620 Wyoming where concentrations are very low.   The % below MDL is very similar for FTIR and IC
621 across the continent. Due to volatility of nitrate, the nitrate metrics for FTIR are poor compared
622 to sulfate (Figure S10-11).

623 ### 3.3.4   PM$_{2.5}$ mass predictions
624 Since the major aerosol species are shown to be reasonably well measured by FT-IR, it was
625 anticipated that PM$_{2.5}$ mass calibration would perform well. The PM$_{2.5}$ model presents reliable
626 filter mass predictions (R^2 = 0.985) characterized by relative bias and error that are 1/3 to 1/2 of
627 those for OC and on par with gravimetric error (Table 1). The cross plot of gravimetric mass and
628 FT-IR predictions (Fig. 4) and maps of predictions metrics (Figure S10-12) show that PM$_{2.5}$ mass
629 can be accurately predicted across a broad concentration range indicating that FT-IR spectra of
630 PTFE filters do not contain interferents or other limitations that make PM mass predictions error
631 prone.

632 ## 3.4   Long term stability
633 Finally, Multilevel calibrations are extended to 2016 and 2017 to evaluate the inter-year
634 consistency and determine if the assumptions behind Limited Sites and Biomass Burning models
635 remain valid over time. For each sampling year, new calibrations were developed following the
636 framework established for 2015. Models were recalibrated with data from the 21 sites and
637 biomass burning samples were detected by the functional group screening procedure. Fig. 6
638 shows the median relative bias (top) and error (bottom) for the three years of data (cross plots
639 and prediction metrics shown for all predicted species for 2016 and 2017 in Section S11). These
640 results indicate that the modeling methodology provided reasonably consistent results across all
641 three years.

642 Normalized bias for most species is below 3% and normalized error is consistent for all species
643 across all three years. The relative bias for EC and BC are similar to other species in 2015 and
644 2017 but in 2016 they are larger in magnitude than the other two years and different in sign.

645 2016 is the first year of TOR data from the multiwavelength TOR instruments (Chow et al., 2015)
646 so higher bias could be potentially be related to the new instruments. However, the HIPS
647 instrument was overhauled beginning in 2017 which provides no explanation for high bias in 2016
648 (http://vista.cira.colostate.edu/improve/Data/QA_QC/Advisory/da0041/da0041_HIPSmodificat
649 ions.pdf). Further, the EC and BC calibrations are independent of each other except for using
650 the same filters for calibrations (as all species do) so the fact that the median bias is roughly equal
651 but opposite in sign is not due to codependence of the models.

652 In future work, calibrations models will be updated more frequently than annually with the most
653 recent year of ambient samples which may smooth biases and errors due to changes to
654 atmospheric condition and instrument drift.
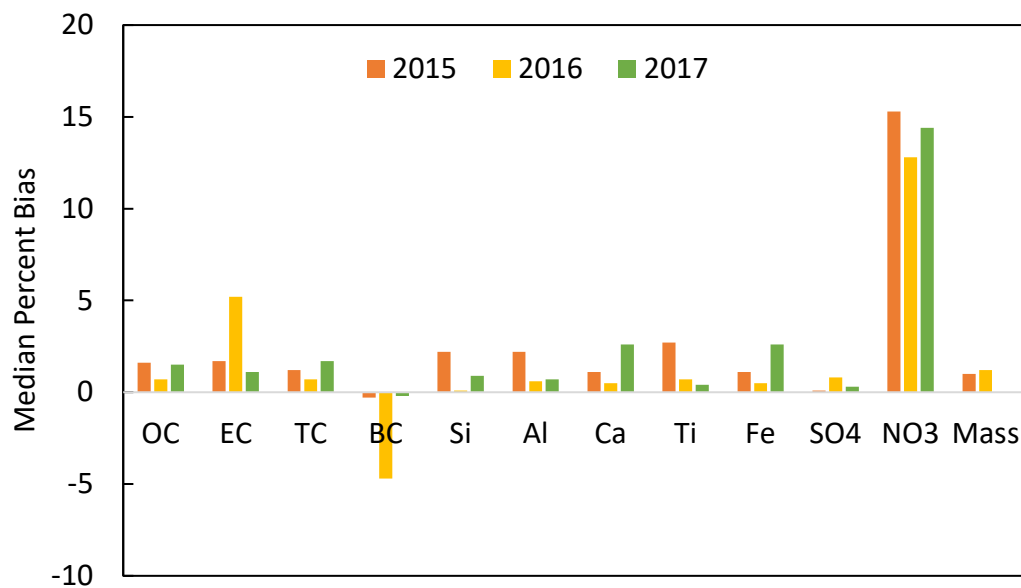
655
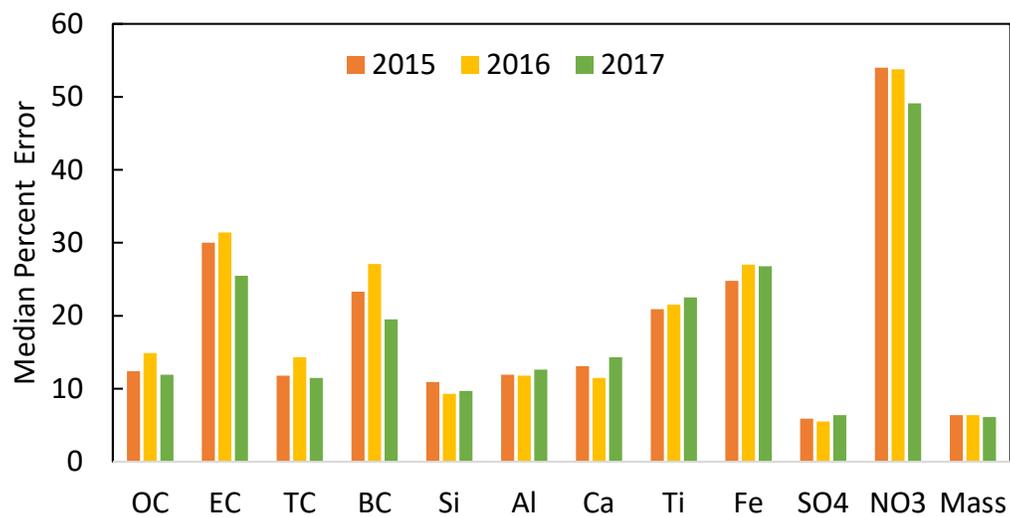
656

657 Figure 6. (top) Median Percent Bias and (bottom) Median Percent Error for each constituent
658 measured for each year.

659

660 4 Conclusion

661 In this paper, we investigate the feasibility of an FT-IR method that uses ambient samples as
662 calibration standards for use by a large monitoring network. In this method, all sites in the

663 network collect PTFE filters for FT-IR analysis. A few select sites, used for calibration, would retain
664 all sampling and analyses of current IMPROVE sites to enable re-calibration of the FTIR method
665 on a routine basis. Re-calibration is especially important as atmospheric changes occur and as
666 conditions in the network evolve over time, for example new reference instruments, new or
667 significantly modified FT-IR instruments, changes to sampling protocol or possibly change in filter
668 material. The validity of such a design was evaluated with all PTFE filters collecting PM$_{2.5}$ aerosols
669 at 161 IMPROVE sites in 2015 and then tested for all filters in 2016 and 2017.

670 A multi-level modeling algorithm was used whereby smoke impacted samples are identified and
671 predicted by one model and the rest of the samples are predicted by another model developed
672 from 21 selected IMPROVE sites. The data from the two models are combined to evaluate
673 performance of the FT-IR method. The selection of sites was performed such that if one of the
674 21 sites ceases to operate, another site, selected from the same compositional cluster can be
675 used for calibration.

676 The cross-plots and prediction metrics indicate that the Multilevel model is equivalent to
677 conventional calibrations built from samples from every available site. Reliable performance in
678 predicted concentrations were reported for a broad range of atmospheric constituents with
679 detectable infrared signatures such as OC, EC, TC, sulfate, soil elements (Si, Al, Ca, Ti, Fe), light
680 absorption, and PM$_{2.5}$ mass. Due to volatilization off the PTFE filter, nitrate measurements were
681 found to be unsatisfactory. The calibration method was develop using data from 2015, and the
682 same methodology was applied to 2016 and 2017. The model performance metrics in all three
683 years were similar. Results across ~61,500 FT-IR spectra highlight the suitability of the Multilevel
684 calibration design to quantify multiple atmospheric PM$_{2.5}$ species in large monitoring networks.

685 This work presents an alternative, lower cost, filter analysis method to measure speciated aerosol
686 in a routine monitoring network. This could be a valuable addition to routine speciated aerosol
687 monitoring networks, such as IMPROVE, by incorporating monitoring sites that collect samples
688 on only a PTFE filter for subsequent analysis. This would provide the opportunity to have a subset
689 of less expensive monitoring site, which could be used for scoping studies to understand the
690 aerosol composition in unmonitored locations. It could also serve as a network cost savings
691 method by having a subset of network sites collect aerosol samples on only a Teflon filter.
692 However, the inability to measure particulate nitrate is a significant deficiency for using this
693 method to replace existing monitoring sites. The FTIR derived aerosol concentrations are also a
694 semi-independent measurement from the routine speciated aerosol measurements. Therefore,
695 routine FTIR measurements would provide valuable QA/QC information for any speciated
696 monitoring network. In addition, FTIR derived concentrations could be used to substitute for
697 missing concentrations in the case where the Teflon sample is valid, but filter samples or analyses
698 on the nylon or quartz fiber filters are not.

699 For IMPROVE's urban counterpart, the CSN network, after evaluation of the quality of
700 predictions in CSN, this framework could be used to accomplish goals similar to those of
701 IMPROVE. Additionally, this method could be used to predict samples collected in the Federal
702 Reference Method (FRM) network which is a PM mass only network. In addition, this method,
703 with appropriate ambient standards, could be applied at other regional or international
704 monitoring networks or sites to provide low-cost comprehensive composition data. As shown
705 in our previous work, additional data, including an estimate of organic matter and it's functional
706 group composition, can also be obtained from FT-IR spectra of PTFE filters, further increasing
707 the utility of infrared spectroscopy of aerosol samples.

5 Data availability

Data is available at https://doi.org/10.25338/B8TP8V.

6 Author contribution

BD developed the software, performed the formal analysis and visualization for much of the manuscript and wrote the original draft of the manuscript, ATW developed software, performed formal analysis and visualization of the GMM work, ST participated in conceptualization, methodology software, visualization and reviewing and editing the manuscript. KMG developed parts of the biomass burning identification methodology. AAF performed the final visualizations for parts of the paper and was responsible for additional visualizations made to the paper based on reviewer comments. BS, SC and ASW, provided input throughout the project and reviewed and edited the manuscript, AMD conceptualized of and acquired funding for this project, developed methodology, performed project administration and supervision and reviewed, edited and finalized the manuscript.

7 Competing interests

The authors declare that they have no conflict of interest.

8 Acknowledgments

The authors acknowledge funding from the National Park Service in cooperation with the Environmental Protection Agency (P18AC01222). Thanks to Anahita Amiri Farahani for assisting with figures. We are particularly grateful to Kelsey Seibert for overseeing daily FT-IR operations at the University of California Davis and to the numerous undergraduate students who performed spectra collection from 2015 to 2017.

9 References

Allen, D. T., Palen, E. J., Haimov, M. I., Hering, S. V., and Young, J. R.: Fourier Transform Infrared Spectroscopy of Aerosol Collected in a Low Pressure Impactor (LPI/FTIR): Method Development and Field Calibration, Aerosol Science and Technology, 21, 325–342, https://doi.org/10.1080/02786829408959719, 1994.

Besalú, E., Julián-Ortiz, J. V. de., Iglesias, M., and Pogliani, L.: An overlooked property of plot methods, Journal of Mathematical Chemistry, 39, 475–484, https://doi.org/10.1007/s10910-005-9035-z, 2006.

Bilmes, J. A.: A gentle tutorial of the EM algorithm and its application to parameter estimation for Gaussian mixture and hidden Markov models, 4:126, 1998.

739 Boris, A. J., Takahama, S., Weakley, A. T., Debus, B. M., Fredrickson, C. D., Esparza-Sanchez, M., Burki, C.,
740 Reggente, M., Shaw, S. L., Edgerton, E. S., and Dillner, A. M.: Quantifying organic matter and functional
741 groups in particulate matter filter samples from the southeastern United States – Part 1: Methods,
742 Atmos. Meas. Tech., 12, 5391–5415, https://doi.org/10.5194/amt-12-5391-2019, 2019.

743 Boris, A. J., Takahama, S., Weakley, A. T., Debus, B. M., Shaw, S. L., Edgerton, E. S., Joo, T., Ng, N. L., and
744 Dillner, A. M.: Quantifying organic matter and functional groups in particulate matter filter samples from
745 the southeastern United States - Part 2: Spatiotemporal trends, 14, 4355–4374,
746 https://doi.org/10.5194/amt-14-4355-2021, 2021.

747 Bro, R. and Smilde, A. K.: Centering and scaling in component analysis, Journal of Chemometrics, 17, 16–
748 33, https://doi.org/10.1002/cem.773, 2003.

749 Burki, C., Reggente, M., Dillner, A. M., Hand, J. L., Shaw, S. L., and Takahama, S.: Analysis of functional
750 groups in atmospheric aerosols by infrared spectroscopy: method development for probabilistic
751 modeling of organic carbon and organic matter concentrations, 13, 1517–1538,
752 https://doi.org/10.5194/amt-13-1517-2020, 2020.

753 Busca, G. and Resini, C.: Vibrational Spectroscopy for the Analysis of Geological and Inorganic Materials,
754 in: Encyclopedia of Analytical Chemistry, John Wiley & Sons, Ltd, 2006.

755 Chow, J. C., Watson, J. G., Pritchett, L. C., Pierson, W. R., Frazier, C. A., and Purcell, R. G.: The dri
756 thermal/optical reflectance carbon analysis system: description, evaluation and applications in U.S. Air
757 quality studies, 27, 1185–1201, https://doi.org/10.1016/0960-1686(93)90245-T, 1993.

758 Chow, J. C., Watson, J. G., Chen, L. W. A., Chang, M. C. O., Robinson, N. F., Trimble, D., and Kohl, S.: The
759 IMPROVE_A Temperature Protocol for Thermal/Optical Carbon Analysis: Maintaining Consistency with a
760 Long-Term Database, 57, 1014–1023, https://doi.org/10.3155/1047-3289.57.9.1014, 2007a.

761 Chow, J. C., Watson, J. G., Chen, L. W. A., Chang, M. C. O., Robinson, N. F., Trimble, D., and Kohl, S.: The
762 IMPROVE_A Temperature Protocol for Thermal/Optical Carbon Analysis: Maintaining Consistency with a
763 Long-Term Database, 57, 1014–1023, https://doi.org/10.3155/1047-3289.57.9.1014, 2007b.

764 Chow, J. C., Wang, X., Sumlin, B. J., Gronstal, S. B., Chen, L.-W. A., Trimble, D. L., Watson, J. G., Kohl, S. D.,
765 Mayorga, S. R., Riggio, G., Hurbain, P. R., Johnson, M., and Zimmermann, R.: Optical Calibration and
766 Equivalence of a Multiwavelength Thermal/Optical Carbon Analyzer, 15, 1145–1159,
767 https://doi.org/10.4209/aaqr.2015.02.0106, 2015.

768 Chukanov, N. V. and Chervonnyi, A. D.: Infrared Spectroscopy of Minerals and Related Compounds,
769 Springer International Publishing, 2016.

770 Cios, K., Pedrycz, W., and Swiniarski, R. W.: Data Mining Methods for Knowledge Discovery, Kluwer
771 Academic Publishers, Norwell, MA, USA, 495 pp., 1998.

772 Corrigan, A. L., Russell, L. M., Takahama, S., Äijälä, M., Ehn, M., Junninen, H., Rinne, J., Petäjä, T.,
773 Kulmala, M., Vogel, A. L., Hoffmann, T., Ebben, C. J., Geiger, F. M., Chhabra, P., Seinfeld, J. H., Worsnop,
774 D. R., Song, W., Auld, J., and Williams, J.: Biogenic and biomass burning organic aerosol in a boreal forest
775 at Hyytiälä, Finland, during HUMPPA-COPEC 2010, 13, 12233–12256, https://doi.org/10.5194/acp-13-
776 12233-2013, 2013.

777 Debus, B., Takahama, S., Weakley, A. T., Seibert, K., and Dillner, A. M.: Long-Term Strategy for Assessing
778 Carbonaceous Particulate Matter Concentrations from Multiple Fourier Transform Infrared (FT-IR)
779 Instruments: Influence of Spectral Dissimilarities on Multivariate Calibration Performance, 73, 271–283,
780 https://doi.org/10.1177/0003702818804574, 2019.

781 Dillner, A. M. and Takahama, S.: Predicting ambient aerosol thermal-optical reflectance measurements
782 from infrared spectra: Elemental carbon, 8, 4013–4023, https://doi.org/10.5194/amt-8-4013-2015,
783 2015a.

784 Dillner, A. M. and Takahama, S.: Predicting ambient aerosol thermal-optical reflectance (TOR)
785 measurements from infrared spectra: Organic carbon, 8, 1097–1109, https://doi.org/10.5194/amt-8-
786 1097-2015, 2015b.

787 Draper, N. R. and Smith, H.: Applied Regression Analysis, 1998.

788 Eldred, Robert. and Ashbaugh, L. L.: Loss of particle nitrate from Teflon sampling filters: Effects on
789 measured gravimetric mass in California and in the IMPROVE network, 54, 93–104,
790 https://doi.org/10.1080/10473289.2004.10470878, 2004.

791 Friedel, R. A. and Carlson, G. L.: Infrared spectra of ground graphite, 75, 1149–1151,
792 https://doi.org/10.1021/j100678a021, 1971.

793 Hahn, A., Vogel, H., Andó, S., Garzanti, E., Kuhn, G., Lantzsch, H., Schüürman, J., Vogt, C., and Zabel, M.:
794 Using Fourier transform infrared spectroscopy to determine mineral phases in sediments, Sedimentary
795 Geology, 375, 27–35, https://doi.org/10.1016/j.sedgeo.2018.03.010, 2018.

796 Hastie, T, Tibshirani, R, and Friedman, J: The Elements of Statistical Learning: Data Mining, Inference,
797 and Prediction, Second Edition, Springer New York, New York, NY, 2009.

798 Hawkins, L. N., Russell, L. M., Covert, D. S., Quinn, P. K., and Bates, T. S.: Carboxylic acids, sulfates, and
799 organosulfates in processed continental organic aerosol over the southeast Pacific Ocean during
800 VOCALS-REx 2008, 115, https://doi.org/10.1029/2009jd013276, 2010.

801 Hyslop, N. P., Trzepla, K., and White, W. H.: Reanalysis of Archived IMPROVE PM2.5 Samples Previously
802 Analyzed over a 15-Year Period, Environ. Sci. Technol., 46, 10106, 2012.

803 Hyslop, N. P., Trzepla, K., and White, W. H.: Assessing the Suitability of Historical PM2.5 Element
804 Measurements for Trend Analysis, Environ. Sci. Technol., 49, 9247–9255,
805 https://doi.org/10.1021/acs.est.5b01572, 2015.

806 Kuzmiakova, A., Dillner, A. M., and Takahama, S.: An automated baseline correction protocol for infrared
807 spectra of atmospheric aerosols collected on polytetrafluoroethylene (Teflon) filters, 9, 2615–2631,
808 https://doi.org/10.5194/amt-9-2615-2016, 2016.

809 Li, H.-D., Xu, Q.-S., and Liang, Y.-Z.: libPLS: An integrated library for partial least squares regression and
810 linear discriminant analysis, 176, 34–43, https://doi.org/10.1016/j.chemolab.2018.03.003, 2018.

811 Liu, S., Ahlm, L., Day, D. A., Russell, L. M., Zhao, Y., Gentner, D. R., Weber, R. J., Goldstein, A. H., Jaoui,
812 M., Offenberg, J. H., Kleindienst, T. E., Rubitschun, C., Surratt, J. D., Sheesley, R. J., and Scheller, S.:
813 Secondary organic aerosol formation from fossil fuel sources contribute majority of summertime organic
814 mass at Bakersfield, 117, https://doi.org/10.1029/2012JD018170, 2012.

815 Madejová, J. and Komadel, P.: Baseline studies of the clay minerals society source clays: Infrared
816 methods, Clays and Clay Minerals, 49, 410–432, https://doi.org/10.1346/CCMN.2001.0490508, 2001.

817 Mahalanobis, P., C,: On the generalized distance in statistics, 2, 49–55, 1936.

818 Malm, W. C., Sisler, J. F., Huffman, D., Eldred, R. A., and Cahill, T. A.: Spatial and seasonal trends in
819 particle concentration and optical extinction in the United States, 99, 1347–1370,
820 https://doi.org/10.1029/93jd02916, 1994.

821 Margenot, A. J., Calderón, F. J., Goyne, K. W., Mukome, F. N. D., and Parikh, S. J.: IR Spectroscopy, Soil
822 Analysis Applications, in: Encyclopedia of Spectroscopy and Spectrometry (Third Edition), edited by:
823 Lindon, J. C., Tranter, G. E., and Koppenaal, D. W., Academic Press, Oxford, 448–454,
824 https://doi.org/10.1016/B978-0-12-409547-2.12170-5, 2017.

825 Mayo, D. W., Miller, F. A., and Hannah, R. W.: Course Notes on the Interpretation of Infrared and Raman
826 Spectra, John Wiley & Sons, Hoboken, NJ, 2004.

827 Nemanich, R. J., Lucovsky, G., and Solin, S. A.: Infrared active optical vibrations of graphite, Solid State
828 Communications, 23, 117–120, https://doi.org/10.1016/0038-1098(77)90663-9, 1977.

829 Ngo, M. A., Pinkerton, K. E., Freeland, S., Geller, M., Ham, W., Cliff, S., Hopkins, L. E., Kleeman, M. J.,
830 Kodavanti, U. P., Meharg, E., Plummer, L., Recendez, J. J., Schenker, M. B., Sioutas, C., Smiley-Jewell, S.,
831 Haas, C., Gutstein, J., and Wexler, A. S.: Airborne particles in the San Joaquin Valley may affect human
832 health, 64, 12–16, https://doi.org/10.3733/ca.v064n01p12, 2010.

833 Niyogi, S., Bekyarova, E., Itkis, M. E., McWilliams, J. L., Hamon, M. A., and Haddon, R. C.: Solution
834 Properties of Graphite and Graphene, 128, 7720–7721, https://doi.org/10.1021/ja060680r, 2006.

O'Dell, K., Ford, B., Fischer, E. V., and Pierce, J. R.: Contribution of wildland-fire smoke to US PM2.5 and its influence on recent trends, 53, 1797–1804, https://doi.org/10.1021/acs.est.8b05430, 2019.

Parks, D. A., Griffiths, P. R., Weakley, A. T., and Miller, A. L.: Quantifying elemental and organic carbon in diesel particulate matter by mid-infrared spectrometry, null, 55, 1014–1027, https://doi.org/10.1080/02786826.2021.1917764, 2021.

Reggente, M., Dillner, A. M., and Takahama, S.: Predicting ambient aerosol thermal-optical reflectance (TOR) measurements from infrared spectra: Extending the predictions to different years and different sites, 9, 441–454, https://doi.org/10.5194/amt-9-441-2016, 2016.

Reggente, M., Dillner, A. M., and Takahama, S.: Analysis of functional groups in atmospheric aerosols by infrared spectroscopy: systematic intercomparison of calibration methods for US measurement network samples, Atmos. Meas. Tech., 12, 2287–2312, https://doi.org/10.5194/amt-12-2287-2019, 2019.

Russell, L. M., Bahadur, R., and Ziemann, P. J.: Identifying organic aerosol sources by comparing functional group composition in chamber and atmospheric particles, 108, 3516–3521, https://doi.org/10.1073/pnas.1006461108, 2011.

Ruthenburg, T. C., Perlin, P. C., Liu, V., McDade, C. E., and Dillner, A. M.: Determination of organic matter and organic matter to organic carbon ratios by infrared spectroscopy with application to selected sites in the IMPROVE network, 86, 47–57, https://doi.org/10.1016/j.atmosenv.2013.12.034, 2014.

Savitzky, A. and Golay, M. J. E.: Smoothing and differentiation of data by simplified least squares procedures, 36, 1627–1639, https://doi.org/10.1021/ac60214a047, 1964.

Schichtel, B. A., Malm, W. C., Bench, G., Fallon, S., McDade, C. E., Chow, J. C., and Watson, J. G.: Fossil and contemporary fine particulate carbon fractions at 12 rural and urban sites in the United States, 113, https://doi.org/10.1029/2007jd008605, 2008.

Senthil Kumar, R. and Rajkumar, P.: Characterization of minerals in air dust particles in the state of Tamilnadu, India through ftir spectroscopy, 2013, 22221–22248, https://doi.org/10.5194/acpd-13-22221-2013, 2013.

Snijders, T. A. B. and Bosker, R. J.: Multilevel Analysis: An Introduction to Basic and Advanced Multilevel Modeling, SAGE, 370 pp., 2011.

Sorooshian, A., Wonaschütz, A., Jarjour, E. G., Hashimoto, B. I., Schichtel, B. A., and Betterton, E. A.: An aerosol climatology for a rapidly growing arid region (southern Arizona): Major aerosol species and remotely sensed aerosol properties, 116, https://doi.org/10.1029/2011jd016197, 2011.

Takahama, S., Schwartz, R. E., Russell, L. M., Macdonald, A. M., Sharma, S., and Leaitch, W. R.: Organic functional groups in aerosol particles from burning and non-burning forest emissions at a high-elevation mountain site, Atmos. Chem. Phys., 11, 6367–6386, https://doi.org/10.5194/acp-11-6367-2011, 2011.

Takahama, S., Dillner, A. M., Weakley, A. T., Reggente, M., Bürki, C., Lbadaoui-Darvas, M., Debus, B., Kuzmiakova, A., and Wexler, A. S.: Atmospheric particulate matter characterization by Fourier transform infrared spectroscopy: a review of statistical calibration strategies for carbonaceous aerosol quantification in US measurement networks, Atmos. Meas. Tech., 12, 525–567, https://doi.org/10.5194/amt-12-525-2019, 2019.

Tuinstra, F. and Koenig, J. L.: Raman Spectrum of Graphite, 53, 1126–1130, https://doi.org/10.1063/1.1674108, 1970.

Watson, J. G. and Chow, J. C.: A wintertime PM2.5 episode at the Fresno, CA, supersite, Atmospheric Environment, 36, 465–475, https://doi.org/10.1016/S1352-2310(01)00309-0, 2002.

Weakley, A. T., Takahama, S., and Dillner, A. M.: Ambient aerosol composition by infrared spectroscopy and partial least-squares in the chemical speciation network: Organic carbon with functional group identification, 50, 1096–1114, https://doi.org/10.1080/02786826.2016.1217389, 2016.

Weakley, A. T., Takahama, S., Wexler, A. S., and Dillner, A. M.: Ambient aerosol composition by infrared spectroscopy and partial least squares in the chemical speciation network: Multilevel modeling for elemental carbon, 52, 642–654, https://doi.org/10.1080/02786826.2018.1439571, 2018a.

Weakley, A. T., Takahama, S., and Dillner, A. M.: Thermal/optical reflectance equivalent organic and elemental carbon determined from federal reference and equivalent method fine particulate matter samples using Fourier transform infrared spectrometry, 52, 1048–1058, https://doi.org/10.1080/02786826.2018.1504161, 2018b.

White, W. H., Trzepla, K., Hyslop, N. P., and Schichtel, B. A.: A critical review of filter transmittance measurements for aerosol light absorption, and de novo calibration for a decade of monitoring on PTFE membranes, 50, 984–1002, https://doi.org/10.1080/02786826.2016.1211615, 2016.

Wold, S., Sjöström, M., and Eriksson, L.: PLS-regression: A basic tool of chemometrics, 58, 109–130, https://doi.org/10.1016/S0169-7439(01)00155-1, 2001.

Yazdani, A., Dudani, N., Takahama, S., Bertrand, A., Prevot, A. S. H., El Haddad, I., and Dillner, A. M.: Characterization of primary and aged wood burning and coal combustion organic aerosols in an environmental chamber and its implications for atmospheric aerosols, 21, 10273–10293, https://doi.org/10.5194/acp-21-10273-2021, 2021a.

Yazdani, A., Dillner, A. M., and Takahama, S.: Estimating mean molecular weight, carbon number, and OM/OC with mid-infrared spectroscopy in organic particulate matter samples from a monitoring network, 14, 4805–4827, https://doi.org/10.5194/amt-14-4805-2021, 2021b.

Zhang, X. L., Trzepla, K., White, W., Raffuse, S., and Hyslop, N. P.: Intercomparison of thermal-optical carbon measurements by Sunset and Desert Research Institute (DRI) analyzers using the IMPROVE_A protocol, 14, 3217–3231, https://doi.org/10.5194/amt-14-3217-2021, 2021.

902